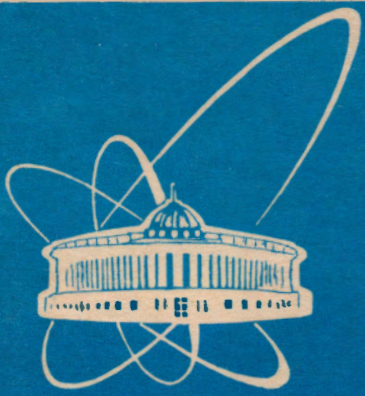

ОБЪЕДИНЕННЫЙ
ИНСТИТУТ
ЯДЕРНЫХ
ИССЛЕДОВАНИЙ

Дубна

95-523

E4-95-523

O.I.Kartavtsev

VARIATIONAL CALCULATION OF ANTIPROTONIC HELIUM ATOMS

Invited talk at the Third Conference on Nucleon-Antinucleon Physics, Moscow, September 11—16, 1995

1995

1 Introduction

The lifetime of negatively charged heavy particles (such as $\pi^-, K^-, \bar{p}$) stopped in matter would be about $10^{-12}s$ due to nuclear absorption after exotic–atom formation. Recently it has been found that a small fraction (a few per cent) of kaons [1], pions [2] and antiprotons [3], [4] stopped in helium media survive for an enormous time (up to tens of microseconds for antiprotons). The reason for this unusual behavior is the formation of a metastable three–body system consisting a helium nucleus, an electron and a negative heavy particle. The prediction of these systems were made as early as thirty years ago by Condo [5] to explain a considerable difference of pion lifetimes in liquid helium and hydrogen. Later on, this qualitative prediction was supported by the variational calculations of Russell [6]. One can mention also the first calculation of the antiprotonic helium atom using the Born-Oppenheimer approximation [7]. Since antiprotons are stable and lifetime of an antiprotonic helium is the largest among these exotic systems, the experimental data concern mainly the antiprotonic helium atom. The modern experiments on the resonant laser-induced annihilation [8, 9] have initiated thorough investigations of these unusual systems. Initial populations, level lifetimes, and very precise values of the transition energies (with a relative accuracy $< 10^{-5}$) have been obtained using this remarkable method.

The antiprotonic helium can be considered as a counterpart of the usual helium atom with one electron replaced by an antiproton. A large angular momentum $L \sim (\mu/m_3)^{1/2}$ (μ is the reduced mass of the antiproton–nucleus subsystem and m_3 is the electron mass) provides that the antiproton-nucleus and electron-nucleus distances are approximately equal. At the same time, this system can be considered as an exotic diatomic molecule, where one nucleus is negatively charged [10].

While there is a number of processes destroying the antiprotonic helium atom, the following considerations explain its very long lifetime. The most part of an extremely large total angular momentum $L \sim 35 - 40$ belongs to the pair of heavy particles and annihilation of an antiproton is inhibited by a large centrifugal barrier. The Auger decay is inhibited due to sufficiently large values ($\lambda_0 \geq 4$) of the angular momentum of an outgoing electron. Usual mechanism of the de-excitation by the Stark mixing is not appropriate for the three-body system due to the lack of degeneracy. The collisional de-excitation by surrounding He atoms is suppressed due to the screening of an antiproton by the electron in an antiprotonic helium. The only remaining de-excitation mechanism is multistep dipole radiative transitions, whose rates of each step are of order μs^{-1}. The discussion of theoretical calculations on antiprotonic helium atoms and related topics can be found in [11].

After the formation of the antiprotonic helium its time evolution is determined by the processes of radiative transition and Auger decay. The precise description of energy spectra requires to take into account the minor effect of relativistic interactions. The spin-dependent part of relativistic interactions gives rise to splitting of energy levels and sufficiently large splitting values can be measured experimentally. The direct variational method provides a possibility in the framework of one approach to calculate eigenenergies, energy-level splitting due to relativistic interactions, radiative transition rates and Auger decay rates of antiprotonic helium atoms. The results of these calculations are presented

and discussed in this report. The isotopic effect is considered by comparison of the calculated properties of $^4He\bar{p}e$ and $^3He\bar{p}e$.

2 Variational method

The nonrelativistic Hamiltonian of the antiprotonic helium atom in the triangular coordinates is

$$H = -\frac{1}{2\mu}\Delta_{\mathbf{r}} - \frac{1}{2\mu_1}\Delta_{\boldsymbol{\rho}} - \frac{1}{m_1}\nabla_{\mathbf{r}}\cdot\nabla_{\boldsymbol{\rho}} - \frac{2}{r} - \frac{2}{\rho} + \frac{1}{|\mathbf{r}-\boldsymbol{\rho}|}, \qquad (1)$$

where $1/\mu = 1/m_1 + 1/m_2$, $1/\mu_1 = 1/m_1 + 1/m_3$ and $m_1, \mathbf{r}_1, m_2, \mathbf{r}_2, m_3, \mathbf{r}_3$ are masses and coordinates of the helium nucleus, antiproton and electron, respectively. Apart from the triangular coordinates $\mathbf{r} = \mathbf{r}_2 - \mathbf{r}_1, \boldsymbol{\rho} = \mathbf{r}_3 - \mathbf{r}_1$, the Jacobi coordinates $\mathbf{r} = \mathbf{r}_2 - \mathbf{r}_1, \boldsymbol{\rho}_1 = \mathbf{r}_3 - (m_1\mathbf{r}_1 - m_2\mathbf{r}_2)/(m_1+m_2)$, corresponding momenta $\mathbf{p} = -i\nabla_{\mathbf{r}}$, $\mathbf{q} = -i\nabla_{\boldsymbol{\rho}}$, $\mathbf{q}_1 = -i\nabla_{\boldsymbol{\rho}_1}$ and angular momenta $\mathbf{l} = [\mathbf{r}\mathbf{p}]$, $\boldsymbol{\lambda} = [\boldsymbol{\rho}\mathbf{q}]$, $\boldsymbol{\lambda}_1 = [\boldsymbol{\rho}_1\mathbf{q}_1]$ will be used to simplify the notation.

Since antiprotonic helium atoms are unstable against the decay to the $He\bar{p} + e$ channel, the variational method cannot be directly applied to the calculation of energies and wave functions. Therefore, according to [12] the approximate Hamiltonian $H_{LN} = P_{LN}HP_{LN}$ which is the projection of the hamiltonian H onto the closed-channel subspace was constructed to calculate the N-th energy level E_{LN} of the system for the total angular momentum L. Explicitly P_{LN} is constructed as a projector onto the subspace of eigenfunctions of relative angular momenta $\mathbf{l}, \boldsymbol{\lambda}$ (or $\mathbf{l}, \boldsymbol{\lambda}_1$), belonging to a limited set of l, λ (or l, λ_1) eigenvalues. While using the Jacobi coordinates this set is defined by the condition $l > l_0$, where l_0 is the largest pair angular momentum satisfying the inequality $\varepsilon_{l_0} < E_{LN}$ and ε_{l_0} is the energy of the hydrogen-like ion $^{3,4}He\bar{p}$ with the angular momentum l_0. If the triangular coordinates are used, this set can be defined by the condition $\lambda < \lambda_0$, where λ_0 is the smallest angular momentum satisfying the inequality $\varepsilon_{L-\lambda_0} < E_{LN}$. By definition, λ_0 is also a multipolarity of the Auger transition, i. e. the smallest angular momentum of the outgoing electron. These conditions describe the natural way to provide the approximate Hamiltonian H_{LN} to have at least N eigenvalues below the boundary of the continuous spectrum and the variational method can be applied to solve the eigenvalue problem for N lowest states of H_{LN}.

It is worthwhile to mention that the $l = L$ projection is the main part of the wave function and the contribution of $l \neq L$ projection rapidly decreases with increasing $|l - L|$. For this reason the approximate Hamiltonian H_{LN} provides an accurate calculation of energies E_{LN} and wave functions Ψ_{LN} for an metastable states ($\lambda_0 \geq 4$) of antiprotonic helium atoms. In fact, the described conditions on l, λ are more restrictive than necessary for an application of the variational method. Practically the accuracy of calculation can be improved taking into account $\lambda > \lambda_0$ (or $l < l_0$ in the case of the Jacobi coordinates) components of the wave function. While using these components a convergence of the calculated values with increasing the number of trial functions will be investigated to provide the reliable results.

3 Energy levels

The variational method described in the previous section was applied to determine eigenfunctions and eigenenergies of the equation

$$(H_{LN} - E_{LN})\Psi_{LN} = 0. \qquad (2)$$

A set of simple variational trial functions of the form

$$\chi^{LM}_{nkl\lambda i}(\mathbf{r}, \boldsymbol{\rho}) = \mathcal{Y}^{LM}_{l\lambda}(\hat{\mathbf{r}}, \hat{\boldsymbol{\rho}}) r^{l+i}\rho^{\lambda} exp(-a_n r - b_k \rho), \qquad (3)$$

where $\mathcal{Y}^{LM}_{l\lambda}(\hat{\mathbf{r}}, \hat{\boldsymbol{\rho}})$ are bispherical harmonics of angular variables, was used in the calculations. It is essential that $\mathcal{Y}^{LM}_{l\lambda}(\hat{\mathbf{r}}, \hat{\boldsymbol{\rho}})$ are eigenfunctions of $\mathbf{l}, \boldsymbol{\lambda}$ and this form of trial functions allows the easy application of the projection method described in Section 2.

Up to 1000 trial functions (3) containing up to 25 bispherical harmonics were used in the calculations. A set of nonlinear parameters a_n, b_k for simplicity was chosen in the form $a_n = a_0\alpha^n, b_k = b_0\beta^k$ and the variation of parameters a_0, α, b_0, β was used to minimize energy values. As it is usual for the variational method, the precision falls down with increasing the excitation number N. To reach more precise energy values, a set of trial functions was limited by the condition $l > L - \lambda_0$ or even less restrictive condition $l > L - \lambda_0 - 1$ instead of $\lambda < \lambda_0$. Convergence of the calculated energies with increasing the number of trial functions was obtained and results are presented in Table 1. Some

Table 1: Calculated energies $E_{LN}(a.u.)$ for five lowest energy levels of the $^{3,4}He\bar{p}e$ systems in the range $31 \leq L \leq 37$

			$^4He\bar{p}e$		
L	E_{L1}	E_{L2}	E_{L3}	E_{L4}	E_{L5}
32	-3.3534091	-3.2272500	-3.1161769	-3.0183048	
33	-3.2158963	-3.1049859	-3.0075402	-2.9219136	-2.8355338
34	-3.0931201	-2.9959130	-2.9107010	-2.8359650	-2.7685835
35	-2.9836255	-2.8988545	-2.8247010	-2.7597140	-2.7007897
36	-2.8862911	-2.8126761	-2.7483976	-2.6920660	-2.6389254
37	-2.7999636	-2.7364076	-2.6809542	-2.6320110	-2.5853018
			$^3He\bar{p}e$		
L	E_{L1}	E_{L2}	E_{L3}	E_{L4}	E_{L5}
31	-3.3484555	-3.2190748	-3.1056452	-3.0061026	
32	-3.2073388	-3.0940418	-2.9949034	-2.9082665	-2.8309327
33	-3.0817523	-2.9829571	-2.8967378	-2.8214095	-2.7539447
34	-2.9702506	-2.8844813	-2.8097982	-2.7445651	-2.7007897
35	-2.8714926	-2.7974268	-2.7330406	-2.6763097	-2.6389254
36	-2.7843183	-2.7207232	-2.6654633	-2.6161392	-2.5853018

information on this calculation can be found also in [12]. Energies of the L, N states of $^4He\bar{p}e$ and $L-1, N$ states of $^3He\bar{p}e$ are very close to each other.

By using the method of laser-induced resonant annihilation, till now, wavelengths of five transitions $(35,4 \to 34,4)$ [8], $(34,3 \to 33,3)$ [13], $(35,2 \to 34,4)$, $(34,3 \to 33,5)$, $(35,3 \to 34,3)$ [14] in $^4He\bar{p}e$ and two transitions $(34,4 \to 33,4)$, $(33,3 \to 32,3)$ [14] in $^3He\bar{p}e$ were measured with high accuracy. The calculated and experimental wavelengths are in agreement with an accuracy not worse than $5 \cdot 10^{-4}$ and more elaborate trial functions are needed to reach a higher accuracy in the energy calculation. Recently, V. I. Korobov has obtained more precise spectra and transition wavelengths of an antiprotonic helium, using the correlated trial functions in variational calculations [15].

4 Radiative transitions

Due to large lifetimes of metastable states against the Auger decay and collisional deexcitation the radiative transitions become the most important to describe the evalution of the antiprotonic helium atom. As far as only dipole transitions are significant, the total angular momentum changes by unity in each transition. Thus, the system looses the angular momentum and energy step-by-step and finally reaches the state with a large Auger decay rate.

The rate of the dipole transition $LN \to L_1N_1$ is given by

$$w = \frac{4}{3(2L+1)} |\alpha(E_{LN} - E_{L_1N_1}|)^3 |M_d|^2 \frac{me^4}{\hbar^3} s^{-1}, \qquad (4)$$

where $\alpha = e^2/\hbar c$ is the fine structure constant and the reduced matrix element of the dipole transition is defined in the form

$$M_d = \langle \Psi_{L_1N_1} || \mathbf{r} + \boldsymbol{\rho} || \Psi_{LN} \rangle. \qquad (5)$$

Variational wave functions Ψ_{LN} and energies E_{LN} have been obtained as described in the previous section and used in (4), (5) to calculate the radiative transition rates. These results are presented in Table 2. A convergence of the calculated values with increasing the number of trial functions provides an estimate of the relative accuracy on the level of one per cent. The radiative transition rates calculated in papers [10], [16], [17] are fairly close to each other and to present results. The important feature is the predominance of transitions between states of the same N, i. e. the approximate conservation of the excitation number in the radiative transitions. Thus, radiative cascades in an antiprotonic helium proceed almost independently along the chains of states of fixed N. However, for higher excitation numbers the probabilities of interchain transitions become more significant and such transitions will be taken into account for the cascade description.

As in the energy calculation, there is a correspondence of the L, N state of $^4He\bar{p}e$ and the $L-1, N$ state of $^3He\bar{p}e$ and the radiative transition rates of the corresponding states are almost the same. At the same time, the $^3He\bar{p}e$ transition rates systematically exceed those of $^4He\bar{p}e$ in accordance with the difference of experimental lifetimes of the antiprotonic helium atoms [4]. However, the explanation of this difference is not simple because the mean lifetime depends also on another processes and a significant difference in populations of the corresponding states was found in the recent experiments for different isotopes [14].

Table 2: Radiative transition rates $w(10^5 s^{-1})$ from the LN to L_1N_1 state of the $^{3,4}He\bar{p}e$ systems. Only transition rates $w \geq 10^4 s^{-1}$ are presented.

$^4He\bar{p}e$				$^3He\bar{p}e$			
transition	w	transition	w	transition	w	transition	w
37,1→36,1	6.733	35,5→34,5	3.143	36,1→35,1	7.255	34,5→33,4	1.036
37,2→36,1	0.159	34,1→33,1	7.744	36,2→35,1	0.187	34,5→33,5	4.532
37,2→36,2	5.859	34,2→33,2	7.554	36,2→35,2	6.255	33,1→32,1	8.483
37,3→36,2	0.441	34,3→33,1	0.206	36,3→35,2	0.511	33,2→32,2	8.240
37,3→36,3	4.907	34,3→33,3	6.926	36,3→35,3	5.182	33,3→32,1	0.301
37,4→36,3	0.742	34,4→33,1	0.288	36,4→35,3	0.887	33,3→32,3	7.539
37,4→36,4	3.990	34,4→33,2	0.137	36,4→35,4	4.135	33,4→32,1	0.476
37,5→36,4	1.218	34,4→33,3	0.355	36,5→35,4	1.642	33,4→32,2	0.205
37,5→36,5	2.947	34,4→33,4	6.073	36,5→35,5	2.934	33,4→32,3	0.387
36,1→35,1	7.249	34,5→33,1	0.355	35,1→34,1	7.846	33,4→32,4	6.577
36,2→35,2	6.531	34,5→33,2	0.365	35,2→34,1	0.102	33,5→32,1	0.748
36,3→35,2	0.333	34,5→33,4	0.728	35,2→34,2	7.019	33,5→32,2	0.571
36,3→35,3	5.644	34,5→33,5	4.840	35,3→34,2	0.384	33,5→32,4	0.807
36,4→35,3	0.637	33,1→32,1	7.720	35,3→34,3	5.995		
36,4→35,4	4.685	33,2→32,2	7.859	35,4→34,3	0.747		
36,5→35,4	1.077	33,3→32,1	0.648	35,4→34,4	4.937		
36,5→35,5	3.323	33,3→32,3	7.492	35,5→34,4	1.304		
35,1→34,1	7.629	33,4→32,1	1.166	35,5→34,5	3.666		
35,2→34,2	7.123	33,4→32,2	0.570	34,1→33,1	8.276		
35,3→34,2	0.205	33,4→32,3	0.151	34,2→33,2	7.700		
35,3→34,3	6.331	33,4→32,4	6.798	34,3→33,2	0.236		
35,4→34,1	0.137	33,5→32,1	3.503	34,3→33,3	6.797		
35,4→34,3	0.509	33,5→32,2	1.537	34,4→33,1	0.169		
35,4→34,4	5.327	33,5→32,3	0.321	34,4→33,3	0.582		
35,5→34,1	0.168	33,5→32,4	0.434	34,4→33,4	5.762		
35,5→34,2	0.187	33,5→32,5	0.730	34,5→33,1	0.199		
35,5→34,4	1.059			34,5→33,2	0.244		

Lifetimes of the $(L,N) = (35,4)$ and $(L,N) = (34,3)$ states of $^4He\bar{p}e$ system were determined experimentally by the method of resonant laser–induced annihilation [9], [13]. Table 3 contains the experimental decay rates and theoretical radiative transition rates of these states. One of the most probable reasons for the difference of experimental and

Table 3: Experimental decay rate and theoretical radiative transition rates ($10^6 s^{-1}$) for two states of the $^4He\bar{p}e$ system

L,N	Experiment	[16]	[10]	present
35,4	0.72 ± 0.02 [9]	0.614	0.619	0.597
34,3	1.18 ± 0.04 [13]	0.734	0.754	0.713

all the theoretical values indicates the substantial contribution of additional nonradiative decay channels. As a density dependence of the lifetime of the (34,3) state in $^4He\bar{p}e$ has been found in recent experiments [14], collisions with surrounding atoms contribute to the decay processes. An extrapolation of the new experimental data to zero density gives $0.91 \pm 0.15 \mu s^{-1}$, which is close to the theoretical radiative transition rate. The density effect probably takes place also for the 35,4 state and the remaining discrepancy may be caused by an additional decay process, e. g. the Auger decay.

5 Energy–level splitting due to relativistic interactions

The precise measurement of transition energies of antiprotonic helium atoms in recent experiments on the laser-induced resonant annihilation [8], [9] invokes the theoretical description of energy spectra with a comparable accuracy. That description of energy spectra requires to take into account the relativistic corrections of an order of α^2 to the pure Coulomb interaction.

Since the contribution to energies from relativistic interactions depends on the antiproton mass, charge and magnetic moment, these calculations can be used for the precise determination of the antiproton properties. This knowledge is essential in testing the fundamental symmetry principles [18].

The spin-dependent part of the relativistic interactions gives rise to splitting of energy levels, and each single transition turns into a multiplet. Sufficiently large distances between lines in the multiplet can be measured experimentally. It is worthwhile to mention that the resolution in current experiments is about 10GHz and without much difficulty can be improved to 1GHz [19]. As it will be discussed below, due to the interaction with electron spin, antiprotonic helium energy levels split into two multiplets and the interaction with nuclei spins provides a minor splitting within each multiplet. Calculation of the former large splitting is discussed in this section. More details of this calculation were presented in [20].

For each pair of particles i,j in the three-body system the relativistic correction of an order of α^2 to the pure Coulomb two-body potential can be described by the Breit interaction $U_{ij}^{(B)}$. The correction to the kinetic energy of an order of α^2 for each particle i is

$$\Delta T_i = -\frac{\alpha^2}{8}\frac{p_i^4}{m_i^3} \qquad (6)$$

Full relativistic correction H_r of an order of α^2 to the three-body nonrelativistic Hamiltonian is a sum of $U_{ij}^{(B)}$ for all pairs of particles and ΔT_i for all particles

$$H_r = \sum_i \Delta T_i + \sum_{i>j} U_{ij}^{(B)}. \qquad (7)$$

In the definition of the expressions $U_{ij}^{(B)}, \Delta T_i$ in eq. (7) it is proposed that particles momenta $\mathbf{p}_i$ will be taken in the center of mass system of three particles [21].

The interaction H_r given in (7) conserves the sum $\mathbf{J} = \mathbf{L} + \sum_i \mathbf{s}_i$ of the total angular momentum $\mathbf{L} = \mathbf{l} + \boldsymbol{\lambda}$ and particle spins $\mathbf{s}_i$. Each level of the nonrelativistic Hamiltonian splits into four and eight sublevels for $^4He\bar{p}e$ and $^3He\bar{p}e$ systems, respectively. Due to very small mass ratios $m_3/m_1, m_3/m_2$, the largest contribution to the energy splitting comes from the interaction with the electron spin $\mathbf{s}_3$. Taking into consideration only terms responsible for the splitting in (7), this part of relativistic interaction can be written as follows:

$$H_s = \alpha^2\Big(\frac{1}{\rho^3}\boldsymbol{\lambda}\mathbf{s}_3 + \frac{1}{2|\mathbf{r}-\boldsymbol{\rho}|^3}[\mathbf{r}-\boldsymbol{\rho},\mathbf{q}]\mathbf{s}_3 - \frac{1}{m_2|\mathbf{r}-\boldsymbol{\rho}|^3}[\mathbf{r}-\boldsymbol{\rho},\mathbf{p}]\mathbf{s}_3 + \frac{2}{m_1\rho^3}[\boldsymbol{\rho},\mathbf{p}]\mathbf{s}_3\Big) \qquad (8)$$

While the last two terms in (8) are inversely proportional to the masses of heavy particle $m_{1,2}$, their contribution to the energy splitting is nevertheless comparable to the contribution from the first two terms for the following reasons. The small mass factor is compensated in part due to the large angular momentum $l \sim L$ of heavy particles. At the same time, only small components of the wave function corresponding to the nonzero electron angular momenta $\lambda \neq 0$ lead to a nonzero splitting value from the first two terms in (8).

The interaction H_s, given in (8), conserves the sum $\mathbf{j} = \mathbf{L} + \mathbf{s}_3$ of the total angular momentum $\mathbf{L}$ and electron spin $\mathbf{s}_3$ and splits each level into two sublevels, corresponding to the eigenvalues $j = L \pm 1/2$. The part of the interaction depending on heavy particle spins removes the remaining degeneracy and splits each $j = L \pm 1/2$ sublevel further into two or four levels for the $^4He\bar{p}e$ and $^3He\bar{p}e$ systems, respectively. Values of this secondary splitting are much smaller in comparison with the splitting arisen due to the interaction with the electron spin (8).

Since the splitting is small in comparison with energy differences between states of different L values, the energy shift Δ_{jLN} for the state with quantum numbers j, L, N can be found in the first order of perturbation theory in H_s

$$\Delta_{jLN} = \langle \Psi_{jLN} | H_s | \Psi_{jLN} \rangle, \qquad (9)$$

where the wave function Ψ_{jLN} of the j, L, N state is the vector production of the nonrelativistic wave function Ψ_{LN} and spin function describing the dependence of the electron spin. Level splitting $\Delta E_{LN} = \Delta_{L+1/2LN} - \Delta_{L-1/2LN}$ is a difference of shifts (9) for $j = L \pm 1/2$.

Due to smallness of the relativistic interaction, radiative transitions proceed only between states of the same j. For this reason, each spectral line of the transition from

the state L_iN_i to state L_fN_f is to be split into a doublet with the interline distance $\Delta\nu = \Delta E_{L_iN_i} - \Delta E_{L_fN_f}$.

Splitting values ΔE_{LN} for a number of states of the $^{3,4}He\bar{p}e$ systems in the range of experimentally observed values of the total angular momentum L have been calculated as described above by using variational nonrelativistic wave functions Ψ_{LN}. These values are presented in Table 4.

Table 4: Splitting values ΔE_{LN} (10^{-6}au) of the lowest levels in the $^{3,4}He\bar{p}e$ systems.

			$^4He\bar{p}e$			
N	L=32	L=33	L=34	L=35	L=36	L=37
1	-1.10	-1.15	-1.15	-1.14	-1.12	-1.09
2	-1.12	-1.09	-1.08	-1.07	-1.04	-1.00
3	-1.01	-1.02	-1.00	-0.98	-0.94	-0.90
4		-0.94	-0.94	-0.90	-0.86	-0.82
5			-0.93	-0.90	-0.84	-0.81
			$^3He\bar{p}e$			
N	L=31	L=32	L=33	L=34	L=35	L=36
1	-1.20	-1.16	-1.19	-1.19	-1.18	-1.14
2	-1.14	-1.19	-1.15	-1.12	-1.08	-1.04
3	-1.08	-1.06	-1.05	-1.04	-1.00	-0.98
4		-0.97	-0.92	-0.86	-0.85	-0.81

As it follows from expression (8), the form of the wave function at small interparticle distances is the most important in evaluating the integral (9). Convergence of the calculated splitting values ΔE_{LN} provides a few per cent relative accuracy. It is worthwhile to mention that due to a better description of the small N states in the variational method, the accuracy of calculation for the L, N state increases with decreasing N. At the same time an accuracy of calculation decreases with decreasing L due to decreasing the multipolarity λ_0 of the Auger decay for large L. Moreover, it is impossible to trace the convergence in the case of short-lived states due to a small multipolarity $\lambda_0 < 3$ of the Auger decay. This problem is closely connected with a large natural width of these states which exceeds significantly a splitting value. Also, the variational procedure meets some difficulties in describing the short range behavior of the wave function for states with large enough N, especially, in the $^3He\bar{p}e$ system. These are the reasons to omit the above-mentioned cases in Table 4.

The last two terms in eq. (8) describe the interaction of the electron magnetic moment with the magnetic field of heavy particles. These terms give rise to the largest contribution to the energy-level splitting. For a better understanding of the splitting dependence on L, N, this contribution is presented in Table 5 for the $^4He\bar{p}e$ system. The contribution to the energy-level splitting from the first two terms in (8) is of opposite sign and smaller in magnitude. Nevertheless, this contribution decreases with increasing L and compensates the L dependence of the last two terms in eq. (8) providing a very slow dependence of the total splitting ΔE_{LN} on L. Due to almost exact conservation of the j value in the radiative transition the spectral line splitting will be found as a difference of ΔE_{LN} presented in

Table 5: Contribution of the last two terms in N_s to the energy-level splitting ΔE_{LN} (10^{-6}au) in the $^4He\bar{p}e$ system.

N	L=32	L=33	L=34	L=35	L=36	L=37
1	-1.41	-1.43	-1.40	-1.37	-1.34	-1.28
2	-1.39	-1.34	-1.30	-1.27	-1.22	-1.16
3	-1.26	-1.24	-1.20	-1.15	-1.10	-1.04
4		-1.14	-1.11	-1.06	-1.00	-0.94
5			-1.10	-1.06	-0.98	-0.95

Table 4. Most appropriate for the experimental measurement are the favoured transitions between states of the same N, which have the largest radiative rates [12], [17], [10]. However, the calculated splitting values are almost independent of L for a given N, and it is not plausible to resolve such a small difference in splitting for the favoured transitions. For this reason, the experimental proposal for the nearest future [19] is aimed at searching for the splitting in unfavoured transitions $(L, N) \to (L-1, N+2)$.

To measure splitting in experiments on the laser-induced resonant annihilation, the initial state should be long-lived. This is provided by the condition that the multipolarity of the Auger decay for this state is $\lambda_0 = 4$. The next condition is that the natural width of the short-lived final state will be smaller than the splitting value, and the multipolarity of the Auger decay for this state will be $\lambda_0 = 3$. The spectral line splitting $\Delta\nu$ for a number of suitable transitions is presented in Table 6. These values are of an order of the

Table 6: Spectral line splitting $\Delta\nu = \Delta E_{L_iN_i} - \Delta E_{L_fN_f}$ (GHz) for the transitions $L_iN_i \to L_fN_f$ in the $^{3,4}He\bar{p}e$ systems.

$^4He\bar{p}e$		$^3He\bar{p}e$	
$L_iN_i \to L_fN_f$	$\Delta\nu$	$L_iN_i \to L_fN_f$	$\Delta\nu$
33,1→32,3	-0.92	32,1→31,3	-0.53
34,1→33,3	-0.86	33,1→32,3	-0.86
34,2→33,4	-0.91	33,2→32,4	-1.22
35,2→34,4	-0.87	34,2→33,4	-1.35
35,3→34,5	-0.34		

experimentally measurable value ~1GHz. One of the recently discovered [14] unfavoured transitions $(35, 2 \to 34, 4)$ in $^4He\bar{p}e$ is a good candidate for the splitting measurement.

Energy-level splitting ΔE_{LN} decreases with increasing the excitation number N and an obvious reason for this dependence is decreasing of the wave function at small interparticle distances for excited states. One can mention an appreciable difference in the ΔE_{LN} dependence on N for the $^4He\bar{p}e$ and $^3He\bar{p}e$ systems. As a consequence, an appreciable isotopic effect appears also for the spectral line splitting $\Delta\nu$.

The following considerations can be used to understand qualitatively the L, N-dependence of the energy-level splitting. The contribution to splitting from the interaction of the electron magnetic moment with the magnetic field of heavy particles is described by the last two terms in the splitting interaction H_s (8). This contribution is

proportional to the relative momentum of heavy particles p. One can consider that the motion of heavy particles is approximately the same as in a hydrogen–like atom and the momentum p is inversely proportional to the angular momentum L. This is the reason for increasing this contribution with decreasing L, as presented in Table 5. The contribution from the first two terms in the splitting interaction H_s is connected with the electron rotation and is proportional to a small component of the wave function arising due to polarization of an electron by an antiproton. With decreasing L the antiproton moves to the region of increasing electron density and the polarization increases. In this way, contributions to the energy–level splitting from the last two terms in H_s and the remaining part of splitting interaction are of opposite sign and level off the dependence of the total splitting ΔE_{LN} on L.

One can consider quasi-classically that the antiproton orbit became more stretched with increasing N at a fixed total angular momentum. For this reason all the terms of the splitting interaction H_s decrease with increasing L and provide the N dependence presented in Tables 4, 6.

6 Auger decay

In addition to the radiative transitions, the important decay channel of antiprotonic helium atoms is the emission of an electron with the $^{3,4}He\bar{p}$ hydrogen-like ion formation, i. e. the Auger decay. The main feature of the Auger decay rates of antiprotonic helium atoms is the essential dependence on the transition multipolarity, i. e. the smallest angular momentum of the outgoing electron λ_0. As discussed in Section 2, calculated eigenenergies E_{LN} [10], [17], [12] unambiguously determine the transition multipolarities λ_0 by the condition $\varepsilon_{L-\lambda_0} < E_{LN}$.

Apart from the early calculation of Russell [6] the only progress in the calculation of the Auger decay rates is due to the paper [16]. It was found that the Auger decay rate decreases about three orders of magnitude with increasing the smallest angular momentum of the outgoing electron λ_0 by one.

As the Auger lifetime of states with $\lambda_0 = 3$ and $\lambda_0 = 4$ is of an order of $10^{-8}s$ and $10^{-5}s$, respectively, and the radiative lifetime is about $10^{-6}s$ [10], [17], [12], the resonant laser-induced transitions between states of $\lambda_0 = 3$ and 4 became observable in the experiments [8], [9]. For this reason, the most important thing is to calculate the Auger decay rates for the states of $^{3,4}He\bar{p}e$ systems with multipolarities $\lambda_0 = 3, 4$. The method and results of the calculation are presented in [22] and will be described in this section. One should mention that there are no other calculations of the Auger decay rate for the $^3He\bar{p}e$ system and the presented results allow one to consider the isotopic effect in this process.

The Auger decay rates of the antiprotonic helium atom are very small in the atomic scale and the very fine details of the discrete state wave functions Ψ_{LN} and continuum wave functions Ψ_c will be accurately determined. In particular, since Ψ_{LN} and Ψ_c belong to the closed- and open-channel subspaces, respectively, the orthogonality condition $\langle\Psi_{LN}|\Psi_c\rangle = 0$ will be strictly fulfilled. As described in Section 2, Ψ_{LN} is an eigenfunction of the approximate Hamiltonian H_{LN} and projector P_{LN}. As a consequence, Ψ_c should be an eigenfunction of the projector $1 - P_{LN}$ and can be found as a solution of the equation

$$(1 - P_{LN})H(1 - P_{LN})\Psi_c = E_{LN}\Psi_c. \tag{10}$$

Thus, the orthogonality requirement is fulfilled and the perturbation theory can be applied due to smallness of the decay rates.

According to the Feshbach orthogonal projection method the decay rate Λ is

$$\Lambda = \frac{1}{\sqrt{2\mu_3(E - \varepsilon_{l_0})}}|M_{tr}|^2\frac{m_3e^4}{\hbar^3}\mathrm{s}^{-1}, \tag{11}$$

where $1/\mu_3 = 1/(m_1 + m_2) + 1/m_3$ and the transition matrix element is

$$M_{tr} = \langle\Psi_c|(1 - P_{LN})HP_{LN}|\Psi_{LN}\rangle. \tag{12}$$

Since the continuum wave function is naturally described in the Jacobi coordinates $\mathbf{r}, \boldsymbol{\rho}_1$, these coordinates will be used in this calculation.

The contribution to M_{tr} is negligible for the Ψ_c components, corresponding to (l, λ_1) eigenvalues of angular momenta $\mathbf{l}, \boldsymbol{\lambda_1}$ if $l \neq l_0, \lambda_1 \neq \lambda_0$. For this reason, only the (l_0, λ_0) component will be taken into account in the calculation of Ψ_c.

Due to the large centrifugal barrier the continuum wave function Ψ_c can be taken as a product of the normalized wave function of $^{3,4}He\bar{p}$ and the function $f(\rho_1)$ describing the relative motion of an electron and $^{3,4}He\bar{p}$. As the total angular momentum of the system is L and its projection is M, Ψ_c takes the form

$$\Psi_c(\mathbf{r}, \boldsymbol{\rho}_1) = A\,\mathcal{Y}^{LM}_{l_0\lambda_0}(\hat{\mathbf{r}}, \hat{\boldsymbol{\rho}}_1)\,r^{l_0}\,e^{-ar}\,f(\rho_1) = \Phi(\mathbf{r}, \hat{\boldsymbol{\rho}}_1)f(\rho_1). \tag{13}$$

In the framework of this approach the interaction of the outgoing electron and the remaining $^{3,4}He\bar{p}$ ion is described by the folding potential

$$V_0(\rho_1) = \langle\Phi|(1 - P_{LN})H(1 - P_{LN})|\Phi\rangle, \tag{14}$$

and the radial function $f(\rho_1)$ obeys the ordinary differential equation.

Due to the large centrifugal barrier for the outgoing electron, the Auger decay rate is mainly determined by the wave functions in the large ρ_1 range, where the interaction of the electron and $^{3,4}He\bar{p}$ system is nearly a sum of the Coulomb and centrifugal potential. Indeed, the replacement of the folding potential by the Coulomb one gives rise to a minor change in the matrix element. This fact supports the applicability of the approximation (13).

500–650 trial functions $\chi^{LM}_{nkl\lambda_1}(\mathbf{r}, \boldsymbol{\rho}_1)$ (3) of the variables $\mathbf{r}, \boldsymbol{\rho}_1$ have been used in the variational calculation of Ψ_{LN}, E_{LN}. As described above, to fulfil the strict requirement of orthogonality, only trial functions satisfying the condition $l > l_0$ have been taken into account. The largest contributions to the transition matrix element M_{tr} come from the $(l, L - l)$ components of the wave function and they have been treated with special care. An additional set of 70–130 trial functions with specific nonlinear parameters have been used to describe these components. As the calculated energy values are in good agreement with the results of [12], one can conclude that the present calculations provide the accurate description of antiprotonic helium atoms. Using Ψ_{LN}, E_{LN} and $\Psi_c(\mathbf{r}, \boldsymbol{\rho}_1)$ in the form (13) the Auger decay rates Λ have been calculated according to equations (11), (12). These results are presented and compared with [16] in Table 7. To understand the role of the wave function structure in this calculation, the largest contributions of the $(l; \lambda_1)$

Table 7: Multipolarities λ_0 and Auger decay rates Λ (s^{-1}) of ^{3,4}Hepe

^{4}Hepe				^{3}Hepe		
L,N	λ_0	Λ	Λ [16]	L,N	λ_0	Λ
34,4	3	$7 \cdot 10^7$	$8.5 \cdot 10^7$	33,4	3	$2 \cdot 10^8$
33,3	3	$1.2 \cdot 10^8$	$1.5 \cdot 10^{8*}$	32,3	3	$3.4 \cdot 10^8$
32,2	3	$1.1 \cdot 10^8$	$4.0 \cdot 10^{7*}$	31,2	3	$3.3 \cdot 10^8$
35,4	4	$\sim 5 \cdot 10^4$	$6.7 \cdot 10^2$	34,4	4	$\sim 10^5$
34,3	4	$\sim 1 \cdot 10^5$	$2.7 \cdot 10^4$	33,3	4	$\sim 10^5$

*K. Ohtsuki, private communication

Table 8: Normalized contributions to the transition matrix element $M_{tr}(l, \lambda_1)$ from the (l, λ_1) components of the wave function for two states of the ^{4}Hepe system.

(L,N)=(34,3) λ_0=4		(L,N)=(34,4) λ_0=3	
(l, λ_1)	$M_{tr}(l, \lambda_1)$	(l, λ_1)	$M_{tr}(l, \lambda_1)$
34,0	-0.28	34,0	0.24
33,1	0.51	33,1	-0.46
32,2	-0.38	32,2	1.22
31,3	1.14		

components of Ψ_{LN} to the transition matrix element are presented in Table 8. It is worthwhile to mention that the exponentially small part of the wave function in the large ρ_1 region is important in evaluating the integral (12). As it follows from the numerical results, the essential point in the calculation of the Auger decay rates is to determine very fine features of the wave function. Really, the largest contribution to the transition matrix element comes from the smallest component corresponding to the largest possible λ_1 value (Table 8) and contributions to the M_{tr} from the (l, λ_1) components of Ψ_{LN} compensate each other due to alternation of signs. Moreover, the most important in the calculation of M_{tr} is the large ρ_1 region of the configuration space, where these components decrease exponentially.

As a result, uncertainty in the calculated decay rates for the multipolarity $\lambda_0 = 3$ is of an order of 10 per cent. As is indicated in Table 7, the decay rates for the $^4He\bar{p}e$ system in this case are in agreement with the results of [16]. The calculated decay rate of the (34,4) state of this system is in fairly good agreement with experimental lifetime τ= 15ns [8]. At the same time, for the (33,3) state the calculated decay rate twice exceeds the experimental value (τ=16.6ns) [13].

On the contrary, the case of the transition multipolarity $\lambda_0 = 4$ is rather complicated for calculation due to much smaller values of the transition matrix element, and only an estimate of the decay rate can be obtained. These values exceed significantly the results obtained in [16].

The calculated decay rates of the $^3He\bar{p}e$ system reveal the substantial isotopic dependence. In fact, decay rates of the (33,4) and (32,3) states of $^3He\bar{p}e$ are about three times as large as those of analogous (34,4) and (33,3) states of $^4He\bar{p}e$. At the same time, other

characteristics of the $(L-1, N)$ state of $^3He\bar{p}e$ are close enough in comparison with the (L, N) state of $^4He\bar{p}e$. As for $\lambda_0 = 4$ transitions of $^3He\bar{p}e$, in this case the calculated decay rates can be estimated only to an order of magnitude and isotope effect is uncertain.

Thus, the Auger decay rates have been calculated for the multipolarities $\lambda_0 = 3, 4$. The method of calculation should be improved to determine with more precision the small components of the wave function and small decay rates in the cases of higher multipolarities $\lambda_0 \geq 4$. Isotopic effect has been found and the role of the structure of the wave function has been studied. The Auger decay rates of metastable states $\lambda_0 = 3$ amount to tenth of the radiative transition rates and can be important in cascade processes. If the isotopic effect for the $\lambda_0 = 3$ states is the same as for $\lambda_0 = 4$ states, the Auger decay in $^3He\bar{p}e$ can compete with radiative transitions.

7 Conclusions

Properties of new three-body systems, the recently discovered antiprotonic helium atoms and analogous hadron–containing systems are intensively investigated both theoretically and experimentally. The investigation of intrinsic properties of antiprotonic helium atoms, their formation and collisions with atoms and molecules is necessary for understanding the antiproton fate in media. The coexistence of a particle and an antiparticle in the same atomic system brings on the principal possibility to study antiproton properties by precise measurements of antiprotonic helium atoms.

Nonstability and an extremely large total angular momentum $L \sim 30 - 40$ of these exotic systems give rise to significant difficulties in the theoretical treatment of this system. However, due to very long lifetimes the metastable states of these systems are treated as true bound states and the variational approach is applied in the calculation. Variational eigenfunctions and eigenenergies are used to obtain the radiative transition rates, energy-level splitting due to relativistic interactions and Auger decay rates of antiprotonic helium atoms. The radiative transitions and Auger decay determine the cascade process after the formation of antiprotonic helium. Calculation of the energy-level splitting will be helpful in the proposed measurement of the multiplet structure [19]. One can mention that these rather different values are sensitive to different parts of the wave function, e. g. the region of small interparticle distances is important in the calculation of energy-level splitting and the asymptotic region is important in the calculation of Auger decay rates.

A simple set of trial functions used in the calculations, nevertheless, provides a description of rather different properties of antiprotonic helium atoms. Convergence of the calculated values with increasing the number of trial functions has been achieved and the isotopic effects have been investigated by comparison of the calculated properties of $^4He\bar{p}e$ and $^3He\bar{p}e$. In this respect, one should mention the investigation of $^6He\bar{p}e$ having in mind that the reduced-mass ratio for $^6He\bar{p}$ and $^4He\bar{p}$ is almost the same as for $^4He\bar{p}$ and $^3He\bar{p}$.

The calculated wave functions can be used also to consider more complicated problems; the most important of them is the determination of formation probabilities and initial populations. Due to substantial density and impurity effects found in experiments [4], [14], [23], other important applications are the interaction of antiprotonic helium atoms with usual helium atoms and diatomic molecules. As for the Auger decay, more efforts are needed to calculate small components of the wave function in the asymptotic

region in cases of higher multipolarities $\lambda_0 \geq 4$.

Acknowledgement. The author is grateful to J. Eades, R. Hayano, K. Ohtsuki, I. Shimamura, E. Widmann and T. Yamazaki for useful discussions and to Computing and Network Division of CERN for the valuable assistance in computations necessary for these calculations.

References

[1] Yamazaki T. e.a., Phys. Rev. Lett., 1989, vol. **63**, p. 1590

[2] Nakamura S. N. e.a., Phys. Rev. A, 1992, vol. **45**, p. 6202

[3] Iwasaki M. e.a., Phys. Rev. Lett., 1991, vol. **67**, p. 1246

[4] Nakamura S. N. e.a., Phys. Rev. A, 1994, vol. **49**, p. 4457

[5] Condo G. T., Phys. Lett., 1964, vol. **9**, p. 65

[6] Russell J. E., Phys. Rev. A, 1970, vol. **1**, p. 721; p. 735; p. 742

[7] Ahlrichs R., Dumbrajs O., Pilkuhn H. and Schlaile H. G., Z. Phys. A, 1982, vol. **306**, p. 297

[8] Morita N. e.a., Phys. Rev. Lett., 1994, vol. **72**, p. 1180

[9] Hayano R. S. e.a., Phys. Rev. Lett., 1994, vol. **73**, p. 1485 (1994); vol.**73**, p. 3181

[10] Shimamura I., Phys. Rev. A, 1992, vol. **46**, p. 3776

[11] Kartavtsev O. I., Few-Body Systems Suppl., 1995, vol. **8**, p. 228

[12] Kartavtsev O. I., Proc. of the 3rd Intern. Symp. on Muon and Pion Interactions with Media, Dubna, 1995, p. 138

[13] Maas F. e.a., Phys. Rev. A, 1995, vol. **52**, p. 4266

[14] Widmann E. e. a., 1995, Proc. of the Third Conference on Nucleon–Antinucleon Physics, Moscow, Yad. Fiz., (in print)

[15] Korobov V. I., Proc. of the Intern. Symp. on Muon Catalyzed Fusion, Dubna, 1995, Hyperfine Interactions (in print)

[16] Morita N., Ohtsuki K. and Yamazaki T., Nucl. Instr. Meth. A, 1993, vol. **330**, p. 439

[17] Yamazaki T. and Ohtsuki K., Phys. Rev. A, 1992, vol. **45**, p. 7782

[18] Charlton M., Eades J., Horvath D., Hughes R. O., Zimmermann C., Phys. Rep. 1994, vol. **241**, p. 65

[19] PS205 Collaboration, 1995, Preprint CERN SPSLC 95-12/SPSLC I 201

[20] Kartavtsev O. I., Proc. of the International Symposium on Exotic Atoms and Nuclei, Hakone, Japan, 1995, Hyperfine Interactions (in print)

[21] Lev F. M., Riv. Nuova Cim. 1993, vol. **16**, p. 1

[22] Fedotov S. I., Kartavtsev O. I., Monakhov D. E., 1995, Proc. of the Third Conference on Nucleon–Antinucleon Physics, Moscow, Yad. Fiz. (in print); JINR Rapid Communications, 1995, No. 5 (73), p. 13

[23] Widmann E. e. a., Phys. Rev. A, 1995, vol. **51**, p. 2870

Received by Publishing Department
on December 21, 1995.

Vacuum (bubble) Feynman integrals (without external momenta) appear as low-energy limits of certain physical amplitudes or as Taylor coefficients of multipoint Green functions. The coefficients can then be used to recover the functions in the whole complex plane of momenta [1]. The presence of virtual heavy particles, like the top quark in the quantum chromodynamics (QCD), generates an effective high-energy scale, which makes perturbation theory applicable owing to asymptotic freedom. In quadratically and linearly divergent diagrams the contributions of heavy particles are enhanced by the power of the mass, so that light particles can well be considered as massless. This leaves us with an important special case of just one nonzero mass.

After performing the Dirac and Lorentz algebra, any vacuum diagram can be reduced to some linear combinations of scalar bubble integrals. In the three-loop case with the full tetrahedron topology of the diagram, all scalar products in the numerator can be expressed through the quadratic combinations in the denominators. Thus, in the most general case, only a product of some powers of the denominators should be integrated. A prototype defines the arrangement of massive and massless lines in a diagram. Individual integrals are specified by the powers of the denominators, called indices of the lines.

In the dimensional regularization with $N = 4 - 2\varepsilon$, any massless bubbles are trivially equal to zero, so that at least one massive line should be present. Fig. 1 displays all possible three-loop prototypes. It was convenient also to distinguish some reduced prototypes with a line missing, E_{2-4}, since they are generated in evaluating several different full prototypes. The B_M and B_N types have been completely analyzed in Ref. [2] and need not be discussed here.

The method of recurrence relations [3, 2] connects integrals of the same prototype but with different values of the indices. Using these relations ingeniously enough, one can reduce any integral to a limited set of so-called master integrals. However, that remains still a kind of art without any strict assertions as to the minimal set of the master integrals or the most efficient strategy. Let us derive a relation [4] for a generic triangle subgraph with masses on its lines m_1, m_2, and m_3, line momenta p_1, $p_2 = p_1 - p_{12}$, and

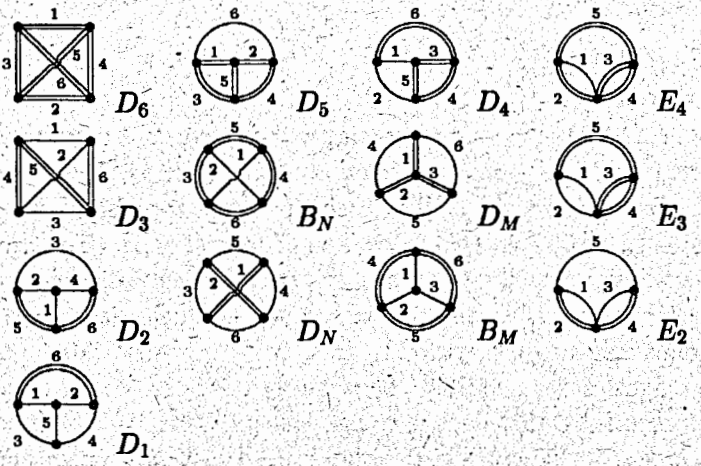

Figure 1: The three-loop scalar bubble prototypes with one mass. Double (single) lines refer to massive (massless) propagators in the momentum representation. Any line may have an integer index, a power of the denominator. The indices stay as arguments of the corresponding functions. Numbers define the ordering of the arguments.

$p_3 = p_1 - p_{13}$, and indices j_1, j_2, and j_3, respectively:

$$0 = \int \mathrm{d}^N p_1 \frac{\partial}{\partial p_1^\mu} \frac{p_1^\mu}{c_1^{j_1} c_2^{j_2} c_3^{j_3}} = \int \frac{\mathrm{d}^N p_1}{c_1^{j_1} c_2^{j_2} c_3^{j_3}} \Big(N - 2j_1 - j_2 - j_3 + j_1 \frac{2m_1^2}{c_1} + j_2 \frac{m_1^2 + m_2^2 - m_{12}^2 + c_{12} - c_1}{c_2} + j_3 \frac{m_1^2 + m_3^2 - m_{13}^2 + c_{13} - c_1}{c_3} \Big), \quad (1)$$

where $c_k = p_k^2 + m_k^2$. Dividing or multiplying by c_k just increments or decrements index j_k of the kth line. The corresponding operator can be denoted by $\mathbf{K}^\pm$ [2]. For an arbitrary L-loop diagram, integrating by parts the first derivatives provides us with L^2 linearly independent relations in total. It is convenient to refer to triangle recurrence relations by specifying only the line numbers: {123} for Eq. (1), line 1 being the base. Half sum of the relations for three faces of a tetrahedron as their base lines form a triangle, like {124}, {534}, and {623} in D_3, gives a relation {dim} that is evident on dimensional grounds:

$$[\tfrac{3}{2} N - j_1 - ... - j_6 + m^2(j_4 \mathbf{4}^+ + j_5 \mathbf{5}^+ + j_6 \mathbf{6}^+)] D_3(j_1, ..., j_6) = 0. \quad (2)$$

Now follows a brief description of evaluating various prototypes. In Fig. 1 they have been ordered from the 'most difficult' to the 'simplest'. Whenever in D_6 a denominator is absent ($j_k \le 0$) the diagram is immediately reduced to the 'simpler' D_5 type by expanding the power of the polynomial. A typical trick to bring any positive index down to 1 is as follows. A combination is sought, like $3\{146\} - \{416\} - \{614\}$ for $j_1 > 1$ in D_6, in which only one 'highest' term $m^2 j_1 \mathbf{1}^+$ is present, all others having the sum of the indices less by one. The highest term can be expressed through the others until the index on the line reaches 1. Thus we arrive at the master integral $D_6(1, ..., 1)$.

If D_5 has $j_5 \le 0$, it is reduced to B_N; $j_{1-4} \le 0$ to D_4. As $j_6 > 0$, it is profitable to solve {612} (no m^2 for a massless exchange between particles of unchanged masses [4]) with respect to the free term. Eventually, this brings $j_{3,4}$ or j_6 to zero. To get rid of the numerator $j_6 < 0$, a denominator on an adjacent line is typically used: if for example $j_1 > 1$, {315} can be solved relative to $\mathbf{1}^+ \mathbf{6}^-$. Otherwise, as $j_{1-4} = 1$, the quadratic denominators can be created by solving {126} with respect to the free term. The irreducible master integral is $D_5(1, 1, 1, 1, 1, 0)$.

In D_4, $j_6 \le 0$ leads to B_M; $j_5 \le 0$ to D_M; $j_{3,4} \le 0$ to D_3; and $j_{1,2} = 0$ to E_4. The numerator on line 1 can be eliminated by {246} if $j_6 > 1$; by $2\{\mathrm{dim}\} - \{534\}$ if $j_3 > 1$; by $\{\mathrm{dim}\} - \{345\}$ if $j_5 > 1$; by $\{\mathrm{dim}\} - \{624\}$ if $j_2 \ne 1$; or by {215} otherwise. Solving {215} relative to $m^2 \mathbf{1}^+$ diminishes the denominator $j_1 > 1$; {512} reduces $j_5 > 1$; $\{435\} - \{534\}$ reduces $j_3 > 1$; $\{136\} + \{246\}$ reduces $j_6 > 1$, leading to $D_4(1, ..., 1)$.

As $j_{4,6} \le 0$ in D_3, this is D_2; $j_5 \le 0 \Rightarrow D_N$; $j_2 \le 0 \Rightarrow B_N$. The numerator $j_1 < 0$ is normally reduced by $2\{\mathrm{dim}\} - \{534\}$ as $j_4 > 1$; by {623} as $j_2 > 1$; by {236} as $j_6 > 1$; by $2\{\mathrm{dim}\} - \{435\}$ as $j_5 > 1$; and {dim} creates $j_{4-6} > 1$ otherwise. The special case $j_1 = j_3 = 0$ is more efficiently worked out as E_4 with $j_5 = 0$. The remaining denominator on line 5 in D_3 is brought down to 1 by {516}; $j_2 > 1$ by $(1 - j_2)\{236\} + j_3 \mathbf{3}^+ \mathbf{2}^- \{326\} + j_6 \mathbf{6}^+ \mathbf{2}^- \{623\}$; and $j_6 > 1$ by $\{156\} - \{534\} + (2 + \mathbf{1}^-/m^2)\{\mathrm{dim}\}$. However, that may revive massless numerators $j_{1,3} < 0$. To avoid infinite loops on recursive application of the relations, we eliminate single numerators by a general projection-operator

method [3]:

$$\int \mathrm{d}^N p_1\ \mathrm{d}^N p_2\ f_1[p_1^2,(p_1-q)^2]\ f_2[p_2^2,(p_2-q)^2]\ A^{2n}(p_1,p_2,q) =$$
$$\frac{\Gamma(n+\frac{1}{2})\,\Gamma[\frac{1}{2}(N-1)]}{\Gamma(\frac{1}{2})\,\Gamma[n+\frac{1}{2}(N-1)]}\prod_{j=1}^{2}\int \mathrm{d}^N p_j\ f_j[p_j^2,(p_j-q)^2]\ A^n(p_j,p_j,q)\,, \qquad (3)$$

where $A(p_1,p_2,q)=4p_1^\mu\,(g_{\mu\nu}-q_\mu q_\nu/q^2)\,p_2^\nu$, and $f_{1,2}$ are arbitrary functions of their scalar arguments. A numerator $[(p_1-p_2)^2]^n$ can be re-expanded:

$$(p_1-p_2)^2=\tfrac{1}{2}\{p_1^2+(p_1-q)^2+p_2^2+(p_2-q)^2$$
$$-[p_1^2-(p_1-q)^2][p_2^2-(p_2-q)^2]/q^2-q^2-A(p_1,p_2,q)\}. \qquad (4)$$

Odd powers of $A(p_1,p_2,q)$ fall out after integration, and for even powers Eq. (3) yields $A(p,p,q)=2[p^2+(p-q)^2]-[p^2-(p-q)^2]^2/q^2-q^2$. For D_3 we identify the left-hand side of Eq. (4) with c_1, and q^2 with c_3. If we deal with $j_1=-1$, $j_3=0$, $j_4=j_6$, then q^2 on the right-hand side of Eq. (4) generates the original integral which can then be eliminated.

The denominator $j_3>1$ is reduced by $\{156\}$–$\{236\}$ while $j_1<0$. At $j_1=0$ with $j_{2,4-6}=1$ we apply $\{236\}$, eliminate $j_1=-1$ by Eqs. (3) and (4), reduce $j_6=2$ as usual, and expand the first numerator again. The original integral with the same value of j_3 can be expressed by solving the resulting equation.

The case $D_3(0,1,1,1,1,1)$ can be transformed as follows. The differential equation for the two-loop subgraph without line 2, Eq. (43) of Ref. [5], is divided by $q^2(q^2+m^2)$ and integrated over q. Derivatives with respect to m^2 are taken via $\{\mathrm{dim}\}$, and after substituting simple integrals we get

$$D_3(0,1,1,1,1,1)=\frac{3N-8}{2m^2}\,D_3(0,1,0,1,1,1)$$
$$+\frac{8\,(m^2)^{3N/2-5}}{(N-2)(N-3)(N-4)^3}\Big[\frac{\Gamma(\frac{1}{2}N-1)\,\Gamma(5-N)}{\Gamma(3-\frac{1}{2}N)}+4\Big]\,, \qquad (5)$$

where each loop integral was divided by $\pi^{N/2}\Gamma(3-\frac{1}{2}N)$; in one loop, this modification agrees with the standard $\overline{\mathrm{MS}}$ definition but is more convenient in higher-loop massive calculations. As a result of the transformations, any D_3-type diagram is reduced to simpler types and two master integrals $D_3(0,1,0,1,1,1)$ and $D_3(1,...,1)$.

With $j_{3,4}\le 0$, E_4 is a particular case of B_M. The numerator on line 5 can be taken off by $\{120\}$ as $j_2>1$ (massless line 0 with index 0 is assumed to connect 1.3 and 2.4); by $\{210\}$ as $j_1\ne 1$; by $\{430\}$ as $j_3>1$; or $\{\mathrm{dim}\}$ should be applied otherwise. The $j_1<0$ numerator is eventually reduced to $j_1=0$ (hence, to the two-loop massive bubbles) by $\{120\}$ if $j_2>1$, or by $\{210\}$. The denominators $j_{1,2}>1$ can be brought down to 1 by solving $\{120\}$ relative to 2^+5^-, or $\{210\}-2m^2 5^+\{120\}$ relative to 1^+5^-. That always increases j_5. The latter helps to reduce the denominators in the massive one-loop subgraph by $2\{340\}-\{430\}$. The extra denominator $j_5>0$ can be integrated off by applying $\{\mathrm{dim}\}$ and reducing $j_2=2$ by $\{120\}$. Iteratively, we arrive at the master integral $E_4(1,1,1,1,0)=D_3(0,1,0,1,1,1)$.

Further prototypes are quite simple indeed. The numerators are manageable by adjacent-triangle relations, and the denominators can be reduced by combining three relations for a triangle that contains the line. The master integrals are $D_M(1,...,1)$, $E_3(1,...,1)$, and $D_N(1,...,1)$. In D_2 the massless relation $\{125\}$ solved with respect to the free term allows one to cancel out a denominator. Thus, in the end D_2 is reduced to Γ functions, just as D_1 does. For E_2 a massless relation can be constructed as $\{524\}-\{\mathrm{dim}\}$.

The described algorithms are implemented as a package of procedures in the symbolic-manipulation language FORM [6] well suited to evaluating the Feynman diagrams as well as any polynomial-like expressions with a large number of terms. However, the efficiency of the essentially recursive programs is restricted by some features of the existing FORM translator. In particular, 'infinitely' iterative substitutions are only allowed without any intermediate sorting of terms. On the other hand, the recurrence relations generate rather many equal terms, and after exceeding certain machine-dependent limits on the size of the scratch expression generated in a module, the sorting becomes extremely slow. The only way out is to use step-by-step sorting inside the preprocessor **#do** loops with a pre-estimated number of repetitions. But sometimes the number is rather difficult to guess at beforehand, while any misjudgement spoils the program performance.

Therefore, it would be highly desirable to implement a kind of the preprocessor **#repeat/endrepeat** construct into FORM, which would terminate as soon as no actual transformations are applicable in any module inside its

body[3]. Also of use would be any means of redefining preprocessor variables, based on global tests on the terms of sorted expressions. An invariable essential inconvenience for structured packages is the global scope of all names in FORM.

The first application of the described package was the evaluation of the three-loop QCD correction to the electroweak ρ parameter [7]:

$$\delta^{QCD} = -\tfrac{2}{3}[1+2\zeta(2)]\,\frac{\alpha_s}{\pi} + \{\tfrac{157}{648} - \tfrac{3313}{162}\,\zeta(2) - \tfrac{308}{27}\,\zeta(3) + \tfrac{143}{18}\,\zeta(4) - \tfrac{4}{3}\,\zeta(2)\ln 2 + \tfrac{441}{8}\,S_2 - \tfrac{1}{9}\,B_4 - \tfrac{1}{18}\,D_3 - [\tfrac{1}{18} - \tfrac{13}{9}\,\zeta(2) + \tfrac{4}{9}\,\zeta(3)]n_f - (\tfrac{11}{6} - \tfrac{1}{9}\,n_f)[1+2\zeta(2)]\ln(\mu^2/m_t^2)\}(\frac{\alpha_s}{\pi})^2, \qquad (6)$$

where α_s is the QCD coupling constant at the renormalization scale μ in the $\overline{\rm MS}$ scheme with the total number of quark flavors n_f (=6); m_t is the pole mass of the top quark; B_4 has been introduced in Ref. [2]; S_2 determines the finite part of the two-loop massive bubble master integral [5]; and D_3 is the finite part of $D_3(1,1,1,1,1,1)$ which has been evaluated numerically by the momentum-expansion method [1] and independently in Ref. [8]. An error in the coefficient of $\zeta(4)$ in the original publication has been fixed, so that Eq. (6) completely agrees with the independent calculation of Ref. [8].

Acknowledgments

I am grateful to the Physics Department of the University of Bielefeld where a part of this work was done. The financial support of Volkswagenstiftung, RFFR grant #94-02-03665, and JSPS FSU Project is thankfully acknowledged. Scientific discussions with O.V. Tarasov were especially useful.

[3] I thank Timo van Ritbergen for informing me that in an wxperimental version of FORM 2.2 it is possible to terminate #do loops as nothing changes. However, this undocumented feature is unavailavle in public versions and, as Jos A.M. Vermaseren communicates, liable to changes in FORM 3

References

[1] J. Fleischer and O.V. Tarasov, *Z. Phys.* **C 64**, 413 (1994); in *Proc. of the* 1994 *Zeuthen Workshop on Elementary Particles, Nucl. Phys. B* (Proc. Suppl.) **37 B**, 115 (1994).

[2] D. Broadhurst, *Z. Phys.* **C 54**, 599 (1992).

[3] K.G. Chetyrkin and F.V. Tkachov, *Nucl. Phys.* **B 192**, 159 (1981); F.V. Tkachov, *Phys. Lett.* **B 100**, 65 (1981).

[4] A.V. Kotikov, *Phys. Lett.* **B 254**, 185 (1991); **B 259**, 314 (1991); **B 267**, 123 (1991).

[5] D.J. Broadhurst, J. Fleischer and O.V. Tarasov, *Z. Phys.* **C 60**, 287 (1993).

[6] J.A.M. Vermaseren, *Symbolic Manipulation with FORM*, Version 2, Tutorial and Reference Manual (Computer Algebra Nederland, Amsterdam, 1991).

[7] L. Avdeev, J. Fleischer, S. Mikhailov and O. Tarasov, *Phys. Lett.* **B 336**, 560 (1994); Erratum **B 349**, 597 (1995); hep-ph/9406363.

[8] K.G. Chetyrkin, J.H. Kühn and M. Steinhauser, *Phys. Lett.* **B 351**, 331 (1995); hep-ph/9502291.

Received by Publishing Department
on December 22, 1995.

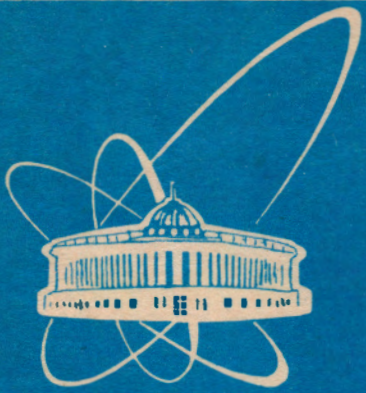

ОБЪЕДИНЕННЫЙ
ИНСТИТУТ
ЯДЕРНЫХ
ИССЛЕДОВАНИЙ

Дубна

95-526

E2-95-526

L.V.Avdeev[1]

RECURRENCE RELATIONS FOR THREE-LOOP PROTOTYPES OF BUBBLE DIAGRAMS WITH A MASS[2]

Submitted to «Zeitschrift für Physik C»

[1]E-mail: avdeevL@thsun1.jinr.dubna.su or avdeevL@hrz.uni-bielefeld.de
[2]Supported in part by Volkswagenstiftung, RFFR grant #94-02-03655, JSPS FSU Project

1995